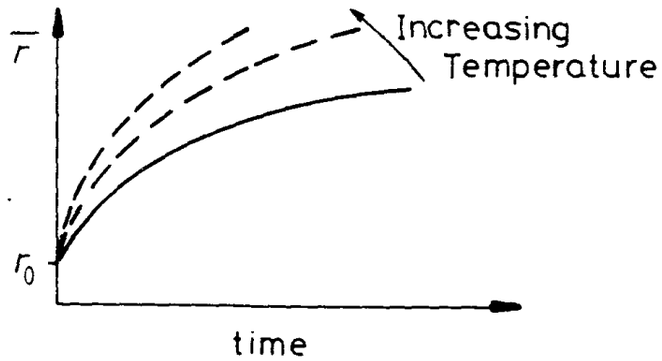

Fig. 5.44 Schematic diagram illustrating how the mean particle radius $\bar{r}$ increases with time at different temperatures.

$$\frac{d\bar{r}}{dt} \propto \frac{k}{\bar{r}^2} \tag{5.52}$$

so that distributions of small precipitates coarsen most rapidly.

In practice the rate at which particles coarsen may not follow a linear r^3–t relationship. Deviations from this relationship can be caused by diffusion short-circuits such as dislocations, or grain boundaries. Also the coarsening rate may be interface controlled. Nevertheless, apart from the case of interface control, the rate of coarsening should depend on the product $D\gamma X_e$, (k in Equation 5.51). Therefore high temperature alloys whose strength depends on a fine precipitate dispersion must have a low value for at least one of γ, X_e or D. Let us consider examples of each of these.

Low γ

The heat-resistant *Nimonic* alloys based on Ni–Cr with additions of Al and Ti obtain their high strength from a fine dispersion of the ordered fcc phase Ni_3(TiAl) (γ') which precipitates in the fcc Ni-rich matrix. The Ni/γ' interfaces are fully coherent and the interfacial energy is exceptionally low (~10–30 mJ m^{-2}) which enables the alloys to maintain a fine structure at high temperature. The misfit between the precipitates and matrix varies between zero and about 0.2% depending on composition. It is interesting that the total creep–rupture life of these alloys can be increased by a factor of 50× by careful control of composition to give zero misfit as compared to 0.2% misfit. The reason for this may be that during creep deformation the particles with the slightly higher misfits lose coherency with the result that γ is increased thereby increasing the rate of coarsening.

Low X_e

High strength at high temperatures can also be obtained with fine oxide dispersions in a metal matrix. For example W and Ni can be strengthened for high temperature use by fine dispersions of thoria ThO_2. In general, oxides are very insoluble in metals and the stability of these microstructures at high temperatures can be attributed to a low value of X_e in the product $D\gamma X_e$.

Low D

Cementite dispersions in tempered steels coarsen very quickly due to the high diffusivity of interstitial carbon. However, if the steel contains a substitutional alloying element that segregates to the carbide, the rate of coarsening becomes limited by the much slower rate at which substitutional diffusion can occur. If the carbide-forming element is present in high concentrations more stable carbides are formed which have the additional advantage of a lower solubility (X_e). Therefore low-alloy steels used for medium temperature creep resistance often have additions of strong carbide-forming elements.

5.6 The Precipitation of Ferrite from Austenite

In this section we will be concerned with phase transformations in which the first phase to appear is that given by the equilibrium phase diagram. The discussion will be illustrated by reference to the diffusional transformation of Fe–C–austenite into ferrite. However, many of the principles are quite general and have analogues in other systems where the equilibrium phases are not preceded by the precipitation of transition phases. Under these conditions the most important nucleation sites are grain boundaries and the surfaces of inclusions.

Consider an Fe–0.15 wt% C alloy which, after austenitizing, is allowed to partially transform to ferrite at various temperatures below A_3 (Fig. 5.45) and then quenched into water. The resultant microstructures are shown in Fig. 5.46. The white areas are ferrite (α). The grey areas are martensite that formed from the untransformed austenite (γ) during quenching. At small undercooling below A_3, Fig. 5.46a, the ferrite nucleates on austenite grain boundaries and grows in a 'blockey' manner to form what are known as grain-boundary allotriomorphs. Note that both smoothly curved, presumably incoherent, α/γ interfaces as well as faceted, semicoherent interfaces are present. At larger undercoolings there is an increasing tendency for the ferrite to grow from the grain boundaries as plates, so-called Widmanstätten side-plates, which become finer with increasing undercooling, Fig. 5.46b, c and d.

Experimental measurements on Widmanstätten ferrite in other ferrous alloys show that the habit planes are irrational, scattered 4 to 20° from $\{111\}_\gamma$, and that orientation relationships close to the Nishiyama–Wasserman or Kurdjumov–Sachs type are usually found. High resolution transmission electron microscopy has also shown that the habit planes have a complex semicoherent structure, containing structural ledges and misfit dislocations, similar to that described in Section 3.4.1[11].

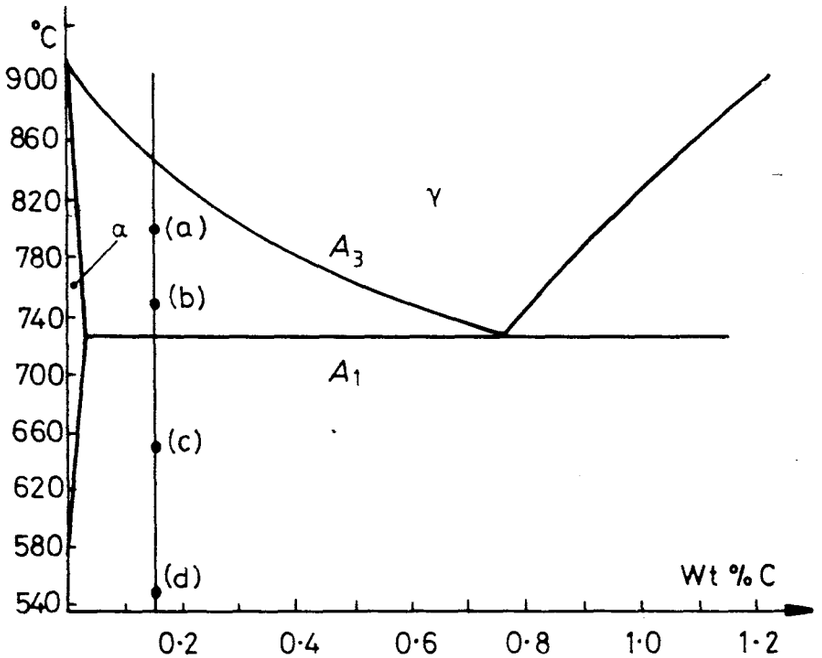

Fig. 5.45 Holding temperatures for steel in Fig. 5.46.

As explained previously, the need to minimize ΔG^* leads to the creation of semicoherent interfaces and orientation relationships, even in the case of grain-boundary nucleation. A critical nucleus could therefore appear as shown in Fig. 3.45b with faceted (planar) coherent (or semicoherent) interfaces and smoothly curved incoherent interfaces. For certain misorientations across the grain boundary it may even be possible for low-energy facets to form with both grains. Due to their low mobility faceted interfaces will tend to persist during growth while incoherent interfaces will be able to grow continuously and thereby retain a smooth curvature. Thus it is possible to explain the presence of smoothly curved and faceted interfaces in Fig. 5.46a.

The reason for the transition from grain boundary allotriomorphs to Widmanstätten side-plates with increasing undercooling is not fully understood. It has been suggested by Aaronson and co-workers[12] that the relative rates at which semicoherent and incoherent interfaces can migrate vary with undercooling as shown in Fig. 5.47. At small undercoolings it is proposed that both semicoherent and incoherent interfaces can migrate at similar rates, while at large undercoolings only incoherent interfaces can make full use of the increased driving force. Consideration of Fig. 5.13 thus shows that approximately equiaxed morphologies should develop at low undercoolings while plate-like morphologies, with ever-increasing aspect ratios, should develop at

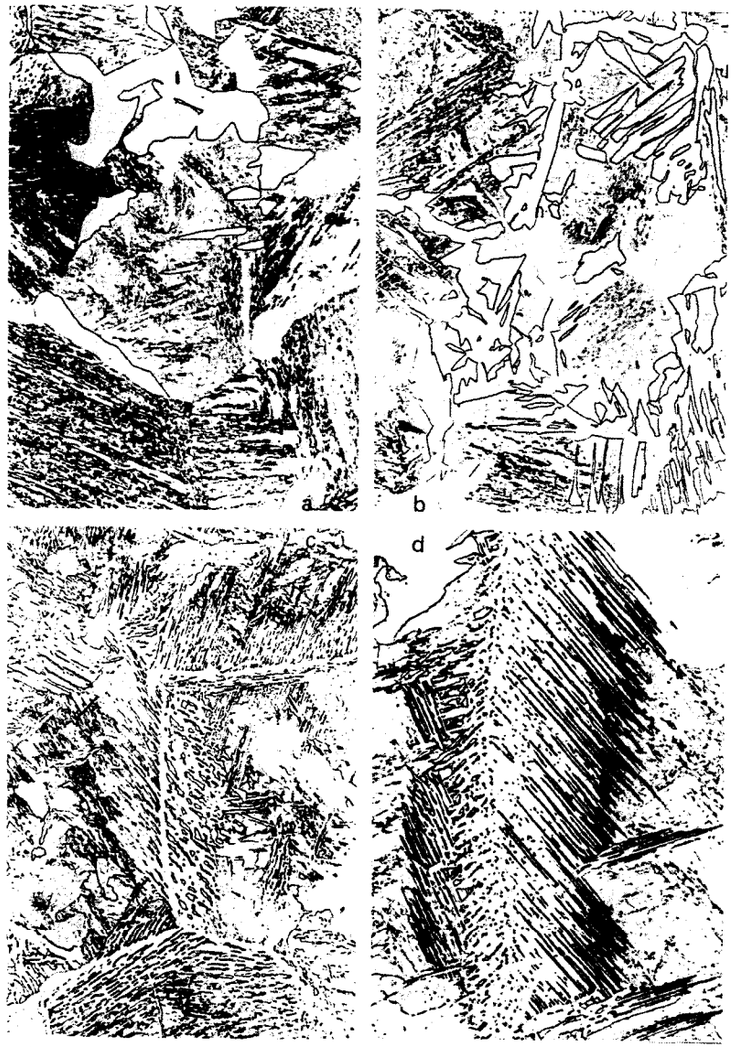

Fig. 5.46 Microstructures of an Fe–0·15% C alloy. The specimens were austenitized, held at an intermediate temperature to give some ferrite, and then quenched to room temperature. The ferrite is white. The grey, fine constituent is a mixture of ferrite and carbide formed on quenching. All photographs are × 100 except (d). (a) 800 °C for 150 s—primarily ferrite allotriomorphs with a few plates. (b) 750 °C for 40 s—many more plates, mostly growing from grain boundaries. (c) 650 °C for 9 s—relatively fine. Note common direction of plates along each boundary. (d) 550 °C for 2 s (× 300) (After P.G. Shewmon, *Transformations in Metals*, McGraw-Hill, New York, 1969, after H.I. Aaronson.)

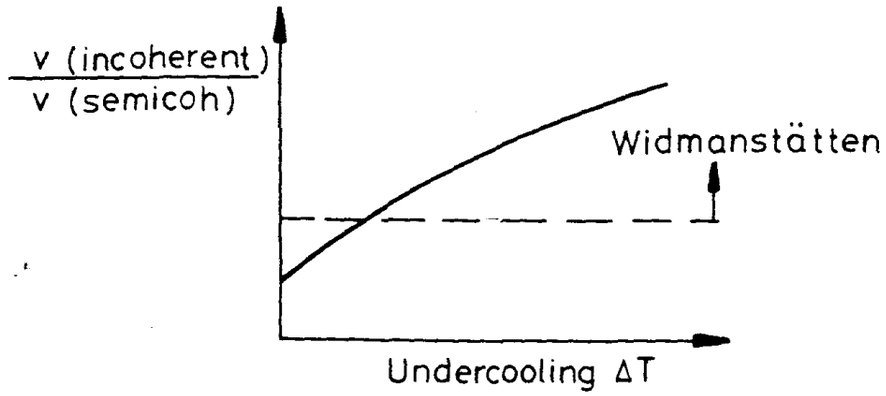

Fig. 5.47 A possible variation of the relative velocity of incoherent and semicoherent interfaces at different undercoolings. Above a certain ratio Widmanstätten morphologies should develop, as shown in Fig. 5.13. (After H.I. Aaronson, in *Decomposition of Austenite by Diffusional Processes*, V.F. Zackay and H.I. Aaronson (Eds.), 1962, by permission of The Metallurgical Society of AIME.)

high undercoolings. Another factor which may contribute to the increased fineness of the Widmanstätten morphologies with decreasing temperature is that the minimum plate-tip radius r^* is inversely proportional to the undercooling.

It can be seen in Fig. 5.46 that ferrite can also precipitate within the austenite grains (intragranular ferrite). Suitable heterogeneous nucleation sites are thought to be inclusions and dislocations. These precipitates are generally equiaxed at low undercoolings and more plate-like at higher undercoolings.

In general the nucleation rate within grains will be less than on grain boundaries. Therefore, whether or not intragranular precipitates are observed depends on the grain size of the specimen. In fine-grained austenite, for example, the ferrite that forms on grain boundaries will rapidly raise the carbon concentration within the middle of the grains, thereby reducing the undercooling and making nucleation even more difficult. In a large-grained specimen, however, it takes a longer time for the carbon rejected from the ferrite to reach the centres of the grains and meanwhile there will be time for nucleation to occur on the less favourable intragranular sites.

A TTT diagram for the precipitation of ferrite in a hypoeutectoid steel will have a typical C shape as shown in Fig. 5.48. The $\gamma \rightarrow \alpha$ transformation should be approximately described by Equation 5.39 and the time for a given percentage transformation will decrease as the constant k increases, e.g. Equation 5.40. As usual, k increases with small increases in T due to increased nucleation and growth rates—k is also raised by an increase in the total number of nucleation sites. Thus decreasing the austenite grain size has the effect of shifting the C curve to shorter transformation times.

It is possible to mark a temperature T_w below which the ferrite forms as predominantly Widmanstätten plates and above which it is mainly in the form

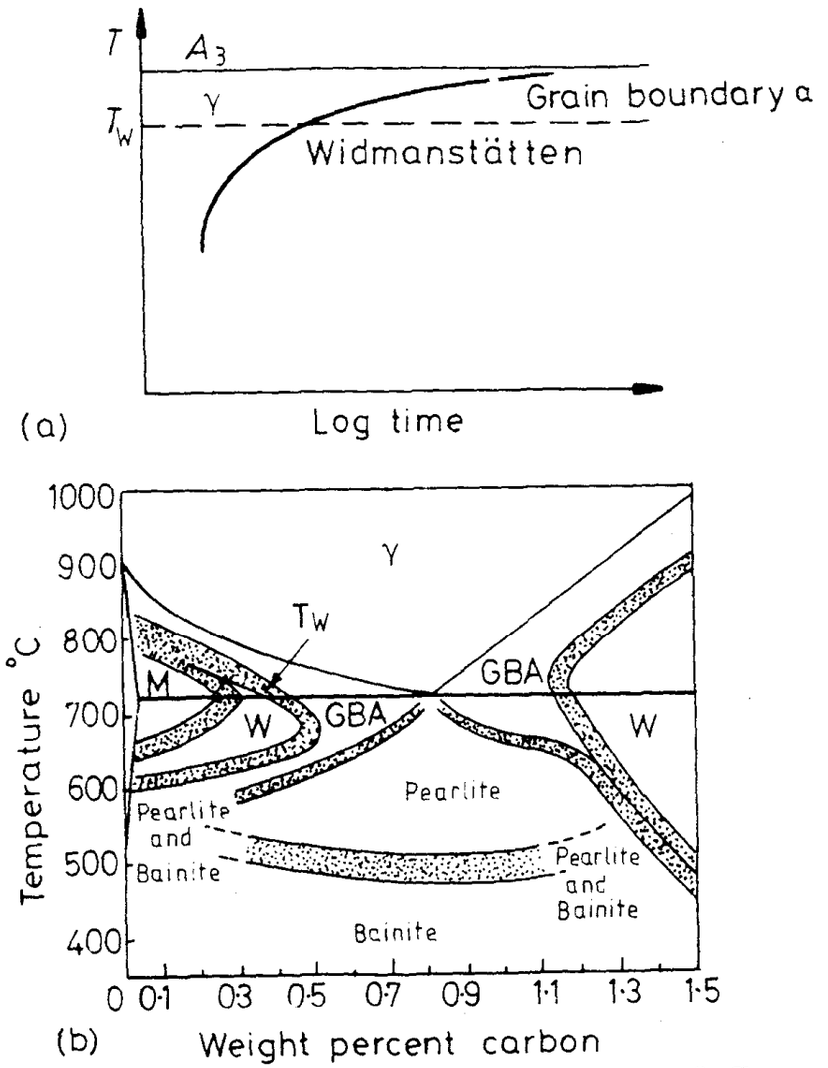

Fig. 5.48 (a) Typical TTT curve for $\gamma \rightarrow \alpha$ transformation. (b) Temperature–composition regions in which the various morphologies are dominant at late reaction times in specimens with ASTM grain size Nos. 0–1. GBA = grain boundary allotriomorphs, W = Widmanstätten sideplates and/or intragranular plates, M = massive ferrite, see Section 5.9. (After H.I. Aaronson, in *Decomposition of Austenite by Diffusional Processes*, V.F. Zackay and H.I. Aaronson (Eds.), 1962, by permission of The Metallurgical Society of AIME.)

of grain boundary allotriomorphs. For alloys of different carbon content A_3 and T_w vary as shown on the phase diagram in Fig. 5.48b.

During practical heat treatments, such as normalizing or annealing, transformation occurs continuously during cooling. Under these circumstances the final microstructure will depend on the cooling rate. If the specimen is cooled

very slowly there will be time for nucleation to occur at small undercoolings on grain corners, edges and boundaries. As these nuclei grow the carbon rejected into the austenite will have time to diffuse over large distances and the austenite grain should maintain a uniform composition given by the equilibrium phase diagram. Finally the austenite reaches the eutectoid composition and transforms to pearlite. Furnace cooling corresponds fairly closely to these conditions and an example is shown in Fig. 5.49c. The final proportions of ferrite and pearlite should be as determined by the equilibrium phase diagram.

The microstructure that results from more rapid cooling will depend on the grain size and the cooling rate. If the rate of cooling is moderately high the specimen will not remain long enough at high temperatures for nucleation to occur. Thus nuclei will not be formed until higher supersaturations are reached. The nucleation rate will then be rapid and large areas of grain boundary will become covered with nuclei. If the temperature is below T_w the ferrite will grow into the austenite as Widmanstätten side-plates with a spacing that becomes finer with decreasing temperature.

The nuclei that form at the highest temperatures will be on grain corners which will be followed by edges at lower temperatures and finally grain boundaries at still lower temperatures. In a *small-grained specimen* where there are a large number of grain corner and edge sites a large number of nuclei can be formed above the T_w temperature and grow as grain-boundary allotriomorphs. In a *larged-grained specimen*, on the other hand, relatively few nuclei will form at high temperatures and the austenite far from these particles will remain supersaturated until lower temperatures, below T_w, when ferrite will be able to nucleate on grain boundary sites and grow as Widmanstätten side-plates. The effect of cooling rate and grain size is illustrated in Fig. 5.49. Note also that the total volume fraction of ferrite decreases as the transformation temperature decreases. This point will be returned to later.

If the austenite contains more than about 0.8wt% C, the first phase to form will be cementite. This also nucleates and grows with an orientation relationship to the austenite, producing similar morphologies to ferrite—grain boundary allotriomorphs at high temperatures and Widmanstätten side-plates at lower temperatures as shown in Fig. 5.48b.

5.7 Cellular Precipitation

Grain-boundary precipitation does not always result in grain-boundary allotriomorphs or Widmanstätten side-plates or needles. In some cases it can result in a different mode of transformation, known as *cellular precipitation*. The essential feature of this type of transformation is that the boundary moves with the growing tips of the precipitates as shown in Fig. 5.50. Morphologically the transformation is very similar to the eutectoid reaction.

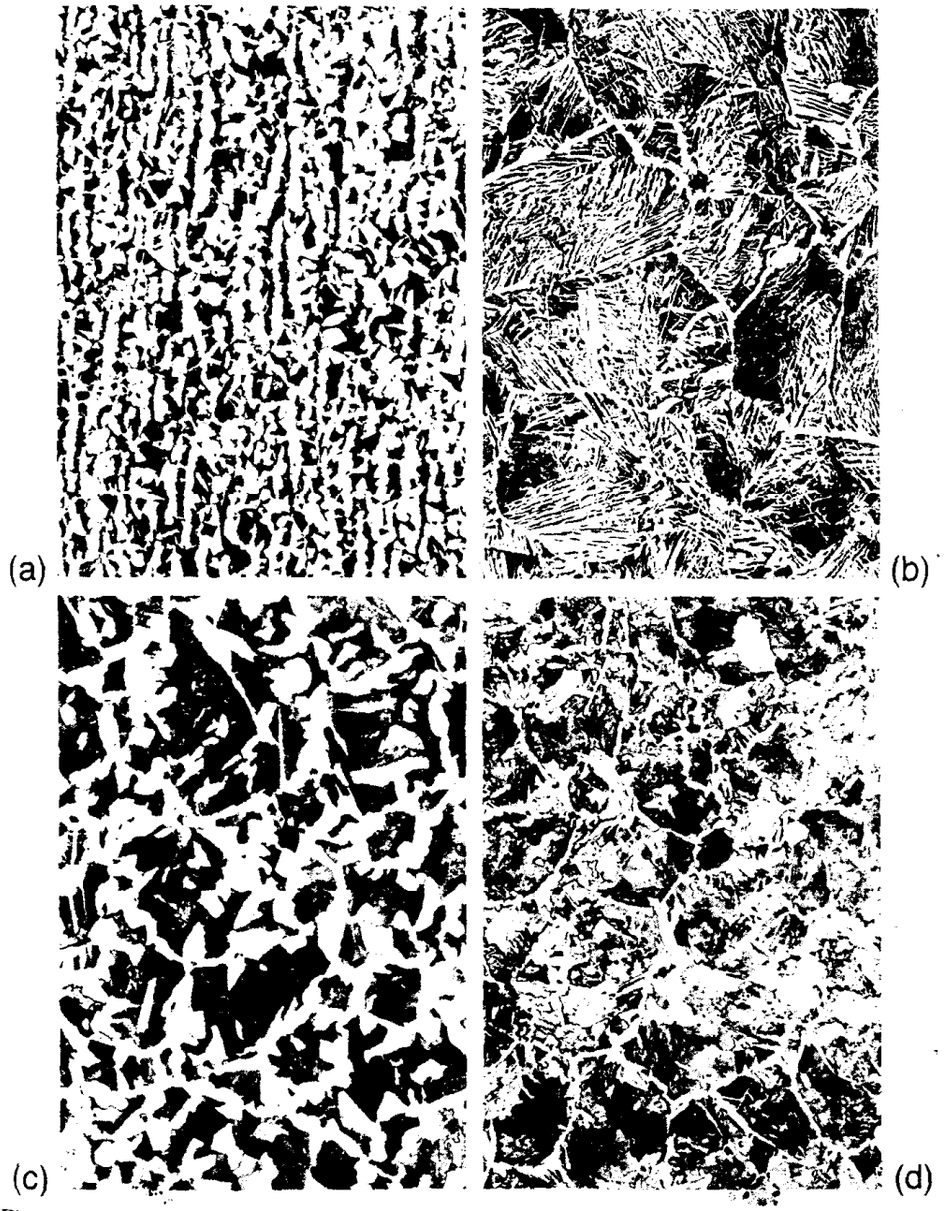

Fig. 5.49 Microstructures obtained from different heat treatments in plain carbon steels (× 60). 0.23wt% C 1.2% Mn air-cooled, showing influence of prior austenite grain size: (a) austenitized at 900 °C (b) austenitized at 1150 °C. 0.4% C showing effect of cooling rate for same grain size: (c) furnace cooled (annealed), (d) air cooled (normalized). (After P.G. Shewmon, *Transformations in Metals*, McGraw-Hill, New York. 1969: (a) and (b) after R. Yoe, (c) and (d) after K. Zurlippe.)

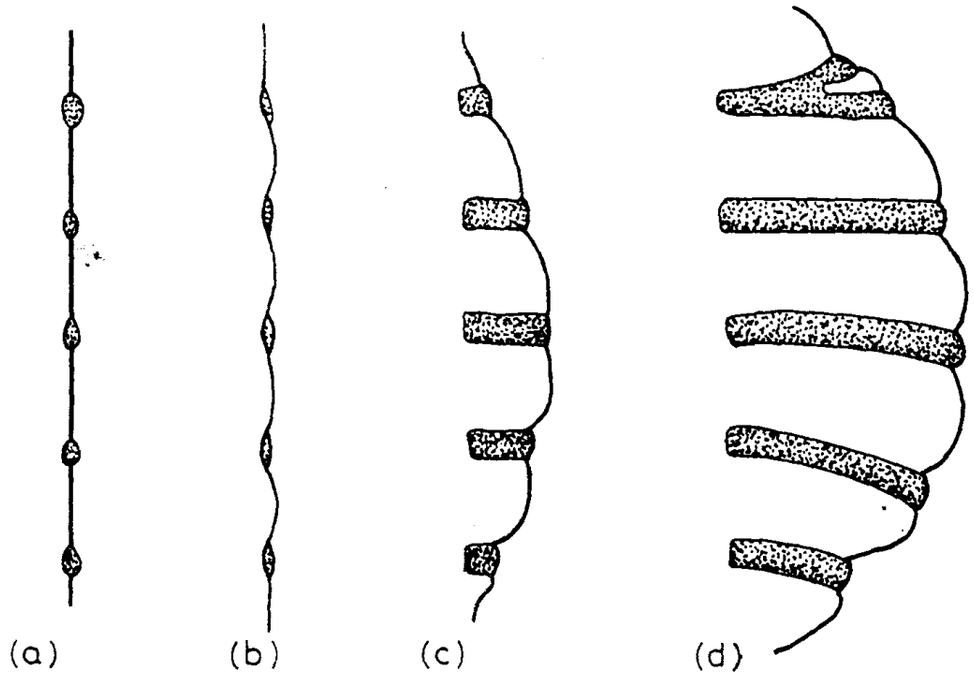

Fig. 5.50 A schematic diagram showing a possible sequence of steps during the development of cellular precipitation.

However, in this case the reaction can be written

$$\alpha' \rightarrow \alpha + \beta$$

where α' is the supersaturated matrix, α is the *same phase* but with a lower thermodynamic excess of solute, and β is the equilibrium precipitate. The mechanism whereby grain-boundary nucleation develops into cellular precipitation differs from one alloy to another and is not always fully understood. The reason why cells develop in some alloys and not in others is also unclear.

Figure 5.51 shows an example of cellular precipitation in a Mg–9 atomic % Al alloy. The β phase in this case is the equilibrium precipitate $Mg_{17}Al_{12}$ indicated in the phase diagram, Fig. 5.52. It can be seen in Fig. 5.51 that the $Mg_{17}Al_{12}$ forms as lamellae embedded in a Mg-rich matrix. The grain boundary between grains I and II was originally straight along AA but has been displaced, and the cell matrix and grain I are the same grain.

Figure 5.53 shows another specimen which has been given a two-stage heat treatment. After solution treating at 410 °C the specimen was quenched to a temperature of 220 °C for 20 min followed by 90 s at 277 °C and finally water quenched. It is apparent that the mean interlamellar spacing is higher at higher ageing temperatures. As with eutectic solidification this is because less free energy is available for the formation of α/β interfaces when the total driving force for transformation is reduced.

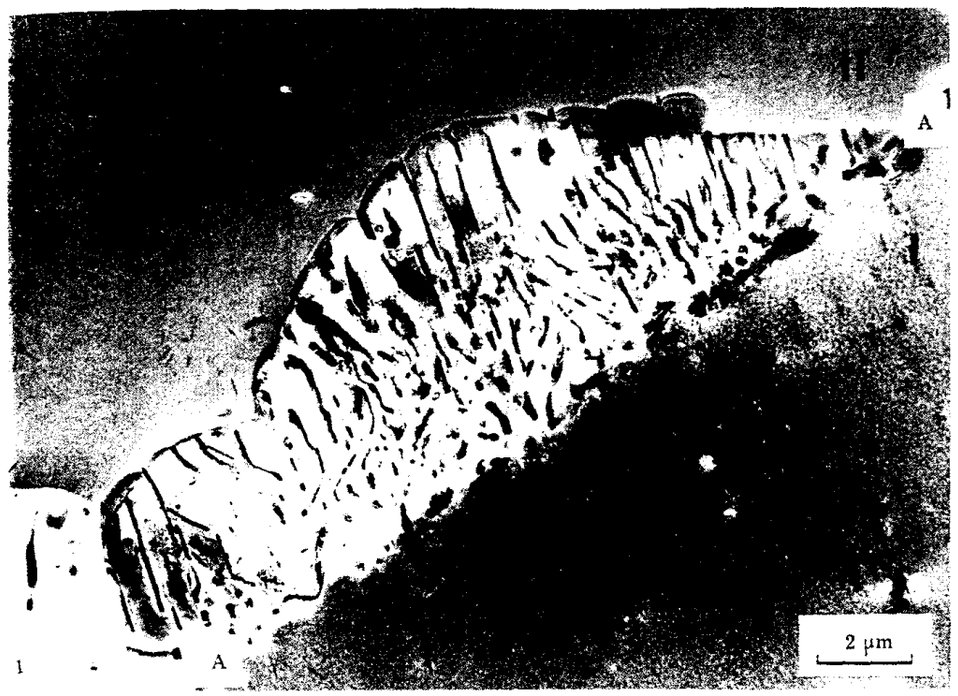

Fig. 5.51 Cellular precipitation of $Mg_{17}Al_{12}$ in an Mg–9 at% Al alloy solution treated and aged 1 h at 220 °C followed by 2 min at 310 °C. Some general $Mg_{17}Al_{12}$ precipitation has also occurred on dislocations within the grains.

The growth of cellular precipitates requires the partitioning of solute to the tips of the precipitates in contact with the advancing grain boundary. This can occur in one of two ways: either by diffusion through the lattice ahead of the advancing cell front, or by diffusion in the moving boundary. Partitioning by lattice diffusion would require solute concentration gradients ahead of the cell front while, if the grain boundary is the most effective diffusion route, the matrix composition should remain unchanged right up to the cell front. In the case of the Mg–Al alloy it has been possible to do microanalysis with sufficiently high spatial resolution to resolve these possibilities directly. (The technique used was electron energy loss spectroscopy using plasmon losses[13].) The results of such measurements, Fig. 5.54a, clearly indicate that the matrix composition remains unchanged to within 10 nm of the advancing cell front so that partitioning must be taking place within the boundary itself. This is to be expected since precipitation is occurring at relatively low temperatures where solute transport tends to become more effective via grain boundaries than through the lattice.

Figure 5.54b shows the aluminium concentration in the α matrix along a line between the β ($Mg_{17}Al_{12}$) lamellae. This is essentially a replica of a similar concentration profile that must exist within the advancing grain boundary. Therefore apart from the matrix in contact with the β precipitate, the cell matrix is still supersaturated with respect to equilibrium.

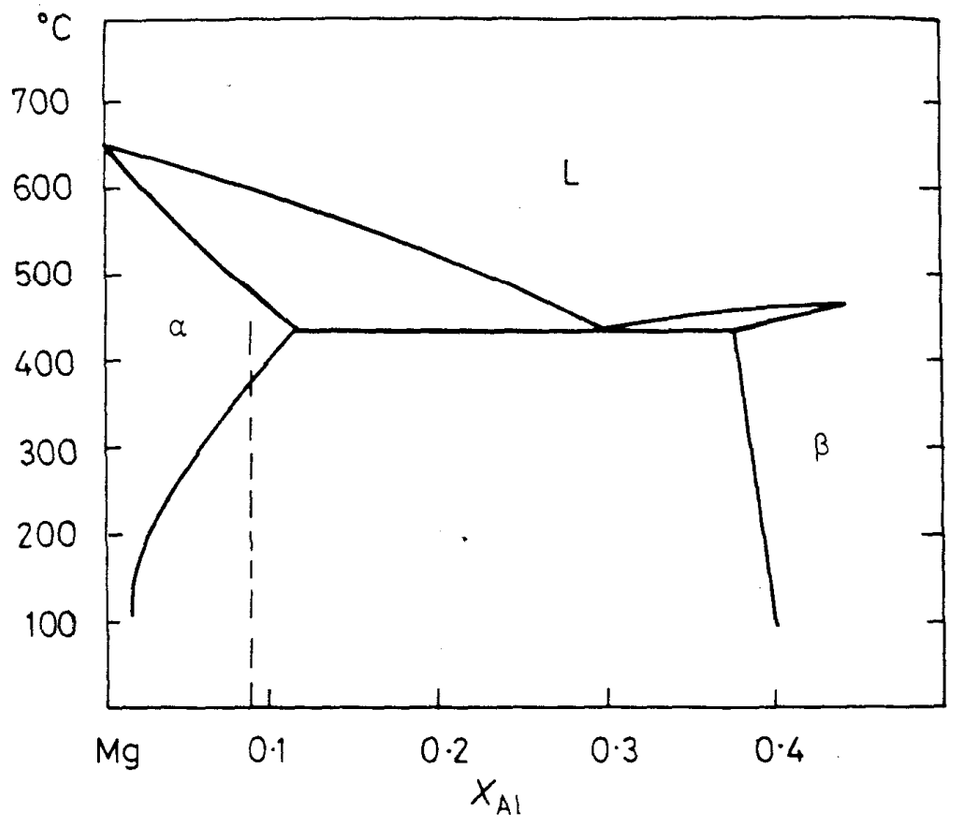

Fig. 5.52 The relevant part of the Mg–Al phase diagram.

Cellular precipitation is also known as *discontinuous precipitation* because the composition of the matrix changes discontinuously as the cell front passes. Precipitation that is not cellular is referred to as general or continuous because it occurs generally throughout the matrix on dislocations or grain boundaries, etc. and the matrix composition at a given point decreases continuously with time. Often general precipitation leads to a finely distributed intermediate precipitate that is associated with good mechanical properties. The cellular reaction is then unwanted because the intermediate precipitates will dissolve as they are overgrown and replaced by the coarse equilibrium precipitates within the cells.

5.8 Eutectoid Transformations

5.8.1 The Pearlite Reaction in Fe–C Alloys

When austenite containing about 0.8wt% C is cooled below the A_1 temperature it becomes simultaneously supersaturated with respect to ferrite and cementite and a eutectoid transformation results, i.e.

$$\gamma \rightarrow \alpha + Fe_3C$$

Fig. 5.53 A cell formed during ageing at two temperatures: 30 min at 220 °C followed by 30 min at 277 °C and water quenched. Note the change in interlamellar spacing caused by the change in undercooling.

The manner in which this reaction occurs is very similar to a eutectic transformation where the original phase is a liquid instead of a solid. In the case of Fe–C alloys the resultant microstructure comprises lamellae, or sheets, of cementite embedded in ferrite as shown in Fig. 5.55. This is known as pearlite. Both cementite and ferrite form directly in contact with the austenite as shown.

Pearlite nodules nucleate on grain boundaries and grow with a roughly constant radial velocity into the surrounding austenite grains. At small undercoolings below A_1 the number of pearlite nodules that nucleate is relatively small, and the nodules can grow as hemispheres or spheres without interfering with each other. At larger undercoolings the nucleation rate is much higher and *site saturation* occurs, that is all boundaries become quickly covered with nodules which grow together forming layers of pearlite outlining the prior austenite grain boundaries, Fig. 5.56.

Nucleation of Pearlite

The first stage in the formation of pearlite is the nucleation of either cementite or ferrite on an austenite grain boundary. Which phase nucleates first will depend on the grain-boundary structure and composition. Suppose that it is cementite. The cementite will try to minimize the activation energy barrier to